International Journal of Microwave and Wireless Technologies

cambridge.org/mrf

Wideband filtering power dividers with wide stopband rejection

Gaoya Dong, Weimin Wang, Bo Zhang and Yuanan Liu

Beijing Key Laboratory of Work Safety Intelligent Monitoring, School of Electronic Engineering, Beijing University of Posts and Telecommunications, P.O. Box 282, Beijing 100876, People's Republic of China

Research Paper

Cite this article: Dong G, Wang W, Zhang B, Liu Y (2019). Wideband filtering power dividers with wide stopband rejection. *International Journal of Microwave and Wireless Technologies* **11**, 7–14. https://doi.org/10.1017/S1759078718001459

Received: 28 May 2018
Revised: 8 October 2018
Accepted: 9 October 2018
First published online: 13 November 2018

Key words:
Coupled line; filtering power divider; wide out-of-band rejection; wide passband

Author for correspondence:
Gaoya Dong, E-mail: gaoyadong@bupt.edu.cn

Abstract

A series of novel wideband filtering power dividers (WFPDs) with wide stopband rejection performances is proposed in this paper. The proposed WFPD structure consists of a parallel-coupled line, two transmission line (TL) sections, four loading terminations, and an isolation resistor. The coupled line is applied at the input port to provide wideband impedance transformation, while different types of loading terminations and TL sections are adopted to realize various out-of-band rejection performances. To verify the proposed concepts, three WFPDs operating at 3.0 GHz are designed and fabricated with 3 dB bandwidth of 79.7, 79.0, and 74.4%. In WFPD1, the measured out-of-band rejection of better than 13.4 dB extends to $2.57f_0$. Moreover, the measured out-of-band rejection of better than 17 dB extends to $2.47f_0$ ($4.75f_0$) in WFPD2 (WFPD3), respectively. Good agreements between the simulated and measured results validate the presented ideas.

Introduction

In modern microwave system, power dividers (PDs) [1] are widely applied in power amplifiers, antenna arrays, mixers, and phase shifters. Bandpass filters are also essential devices in radio frequency and microwave front ends. Conventionally, the PDs and bandpass filters are usually cascaded to provide signals splitting and filtering performances simultaneously. However, the cascades of PDs and bandpass filters will lead to relative high insertion losses and bulky circuit sizes. To overcome such shortcomings, filtering PDs have been investigated in [2–19] which can achieve signals splitting and filtering performances simultaneously in only one device.

In addition, wide upper stopband frequency range with deep rejection level is greatly demanded to suppress the out-of-band interferences, i.e. background noises and intermodulation signals from non-linear components, which commonly exist in modern communication system. Recently, some narrowband PDs with high passband selectivities and good out-of-band rejection performances are proposed in [2–9]. In [2], a low-pass filter is inserted into the PD to realize harmonic suppression. Stub resonators introduced in [3–5] and composite right-/left-handed transmission line (TL) structures employed in [6] could generate transmission zeros (TZs), resulting in filtering responses and wide upper stopband ranges with high attenuations. In [7–9], filtering PDs with good out-of-band rejection performances have been designed based on coupling structures. Unfortunately, the 3 dB fractional bandwidths (BWs) of the PDs mentioned in [2–9] are all <12%, which makes them not suitable for wideband communication systems.

With the development of wideband communication systems, it is essential to enhance the BW of filtering PDs. Some wideband filtering PDs (WFPDs) have been presented in [10–19]. Coupling topology between a quarter-wavelength short-ended microstrip TL and two multimode resonators is introduced in [10] to design WFPD with the 3 dB fractional BW of 32.1%. In [11], a WFPD with 3 dB fractional BW of 109.5% is achieved by adopting parallel-coupled lines and a pair of quarter-wavelength short-circuited stubs. Periodic butterfly radial slots are etched on top layer of substrate-integrated waveguide in [12] to realize a WFPD with 3 dB fractional BW of 44.4%. In [12], the upper stopband extends to $1.78f_0$ with the attenuation of 26 dB, which is the best out-of-band rejection performance among the WFPDs presented in [10–12]. However, the poor out-of-band rejection performance will limit the application of such devices in multi-standard wireless communication systems. Some efforts [13–19] have also been made to design wideband PDs (WPDs) with filtering responses, wide upper-stopband range as well as deep rejection levels. In [13], by replacing quarter-wavelength TLs in conventional Wilkinson PD with filters, a WPD with passband selectivity and harmonic suppression performances is realized. Coupled lines and loading terminations are adopted in [14–19] to design WPDs with filtering responses and good out-of-band rejection performances. The WPD proposed in [19] achieves the best out-of-band rejection performance among the structures presented in [10–19], where the upper stopband extends to $5.0f_0$ with a rejection level of 17.2 dB. However, the passband selectivity of WPD proposed

© Cambridge University Press and the European Microwave Association 2018

CAMBRIDGE UNIVERSITY PRESS

in [19] needs to be further enhanced. The WPDs in [13–18] have high passband selectivity performances, but the harmonic suppression performances should be further improved.

In this paper, a series of novel wideband PDs with various TL sections and loading terminations is proposed to realize high passband selectivities and good out-of-band rejection performances. The operating mechanisms of the basic WFPD circuit are explained in detail based on the even-odd mode method. Three WFPDs are designed, fabricated, and measured to verify the proposed ideas.

Analysis of basic WFPD circuit

Figure 1(a) depicts the schematic representation of the basic WFPD circuit, which consists of a parallel-coupled line, two aligned TL sections, four loading terminations (Z_{T1}, Z_{T1}, Z_{T2}, Z_{T2}), and an isolation resister (R). The even-mode equivalent circuit and the odd-mode equivalent circuit of the proposed basic WFPD circuit are shown in Figs 1(b) and 1(c), respectively. Define the source (load) impedance as $Z_S(Z_L)$ and $Z_{T1} = jX_{T1}$, $Z_{T2} = jX_{T2}$. As observed in the even-mode equivalent circuit, the ABCD matrix of section A_e can be deduced as equation (1), and the expression of $Z_{eq,in}$ could be derived as equation (2).

$$\begin{pmatrix} A_{em} & B_{em} \\ C_{em} & D_{em} \end{pmatrix} = \begin{pmatrix} 1 & 0 \\ \frac{1}{jX_{T1}} & 1 \end{pmatrix} \begin{pmatrix} A_{TL} & B_{TL} \\ C_{TL} & D_{TL} \end{pmatrix} \begin{pmatrix} 1 & 0 \\ \frac{1}{jX_{T2}} & 1 \end{pmatrix}, \quad (1)$$

$$Z_{eq,in} = \frac{X_{T1}(X_{T2}F - jB_{TL}Z_S)}{2(X_{T1}X_{T2}E - jX_{T2}F - (jX_{T1}D_{TL} + B_{TL})Z_S)}, \quad (2)$$

where $E = C_{TL}Z_L + D_{TL}$,

$$F = A_{TL}Z_L + B_{TL}.$$

As observed from Fig. 1(b), the terminal conditions of the four-port coupled lines can be expressed as equation (3). According to equation (3) and four-port impedance matrix of the coupled line shown in paper [20], the input impedance in port 1 (Z_{INE}) can be calculated as equation (4). Thus, the reflection coefficient (S_{11}) and the transmission coefficient (S_{21}) can be extracted as equation (5).

$$I_1 = I_3 = 0, \quad (3a)$$

$$V_4 = -Z_{eq,in} \cdot I_4, \quad (3b)$$

$$Z_{INE} = \frac{(Z_e - Z_o)^2 \csc^2\theta}{4Z_{eq,in} - (Z_e + Z_o)^2 \cot^2\theta} - \frac{(Z_e + Z_o)^2 \cot^2\theta}{4}, \quad (4)$$

$$S_{11} = \left| \frac{Z_{INE} - Z_S}{Z_{INE} + Z_S} \right|, \quad (5a)$$

$$S_{21} = \sqrt{1 - \left(\frac{Z_{INE} - Z_S}{Z_{INE} + Z_S} \right)^2}. \quad (5b)$$

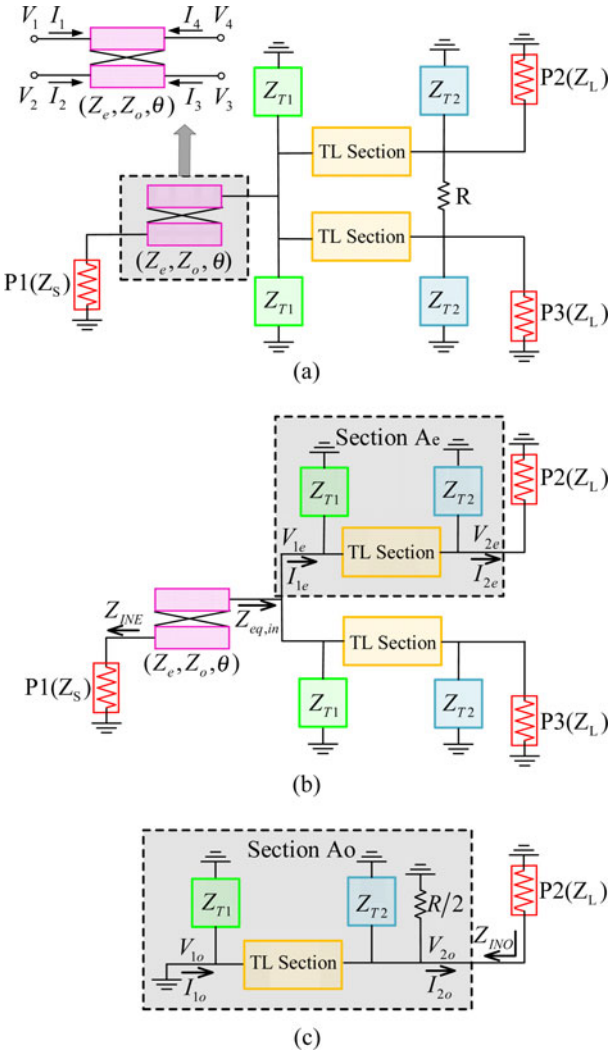

Fig. 1. Proposed WFPD circuit. (a) The schematic representation. (b) Even-mode equivalent circuit. (c) Odd-mode equivalent circuit.

According to the odd-mode equivalent circuit shown in Fig. 1(c), the ABCD matrix of section A_o could be expressed as equation (6), and input impedance in port 2 (Z_{INO}) can be expressed as equation (7). Thus, the return loss in port 2 (S_{22}) could be deduced as equation (8).

$$\begin{pmatrix} A_{om} & B_{om} \\ C_{om} & D_{om} \end{pmatrix} = \begin{pmatrix} A_{TL} & B_{TL} \\ C_{TL} & D_{TL} \end{pmatrix} \begin{pmatrix} 1 & 0 \\ \frac{1}{jX_{T2}} & 1 \end{pmatrix} \begin{pmatrix} 1 & 0 \\ \frac{2}{R} & 1 \end{pmatrix}, \quad (6)$$

$$Z_{INO} = \frac{Z_{2o}}{I_{2o}} = \frac{B_{TL}}{A_{TL} + \frac{B_{TL}}{jX_{T2}} + \frac{2B_{TL}}{R}}, \quad (7)$$

$$S_{22} = \left| \frac{Z_{INO} - Z_L}{Z_{INO} + Z_L} \right|. \quad (8)$$

Two kinds of TL sections, i.e. (1) quarter-wavelength TL and (2) dual TLs (DTLs) are demonstrated in Fig. 2, which could be adopted to replace the TL section in the basic WFPD circuit.

https://doi.org/10.1017/S1759078718001459 Published online by Cambridge University Press

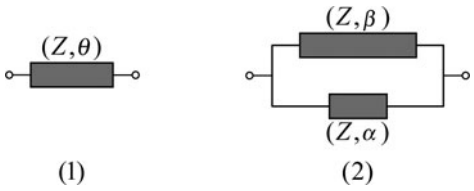

Fig. 2. Two kinds of transmission line sections.

Three types of loading terminations, i.e. (3) short-circuited stub, (4) cascade open-circuited stub, and (5) short-circuited DTLs stub shown in Fig. 3 could be employed as the practical realization of Z_{T1} and Z_{T2}. Various types of WFPDs can be designed with different TL sections and loading terminations.

Analysis of specific WFPDs

In this section, the signals splitting and signals filtering performances of three different WFPDs are analyzed under even-mode excitation. Then, isolation performances are explained under odd-mode excitation.

Analysis of WFPD1 under even-mode excitation

For WFPD1, the loading termination Z_{T1} is selected as (3) short-circuited stub and the loading termination Z_{T2} is implemented as (4) cascade open-circuited stub, while TL section is chosen as (1) quarter-wavelength TL. Based on the schematic representation of WFPD1 shown in Table 1, ABCD parameters of the (1) quarter-wavelength transmission, X_{T1} and X_{T2} could be expressed as equation (9).

$$\begin{pmatrix} A_{TL} & B_{TL} \\ C_{TL} & D_{TL} \end{pmatrix} = \begin{pmatrix} \cos\theta & jZ_1 \\ jY_1 & \cos\theta \end{pmatrix}, \tag{9a}$$

$$X_{T1} = Z_2 \tan\theta, \tag{9b}$$

$$X_{T2} = \frac{Z_4 \cot\theta(\tan^2\theta - Z_3/Z_4)}{1 + Z_3/Z_4}, \tag{9c}$$

$$Z_{INE} = \frac{(Z_e - Z_o)^2 Z_L}{2Z_1^2}, \tag{10}$$

$$f_{TZ0} = 0, \tag{11a}$$

$$f_{TZ1} = \frac{2f_0}{\pi}\arctan\sqrt{Z_3/Z_4}, \tag{11b}$$

$$f_{TZ2} = 2f_0 - \frac{2f_0}{\pi}\arctan\sqrt{Z_3/Z_4}, \tag{11c}$$

$$f_{TZ3} = 2f_0. \tag{11d}$$

At f_0, $A_{TL} = D_{TL} = 1/X_{T1} = 1/X_{T2} = 0$. Combining equations (4) and (9), the input impedance in port 1 (Z_{INE}) could be calculated as equation (10) when WFPD1 is under even-mode excitation.

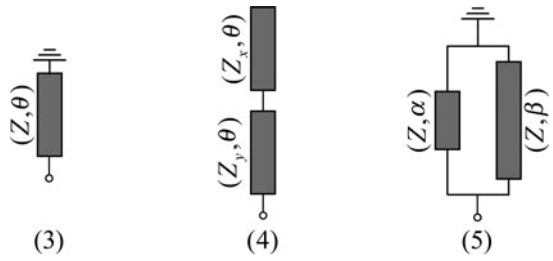

Fig. 3. Three kinds of loading terminations.

According to equations (1–5) and (9), the expressions of TZs could be derived as equation (11), which agrees well with the normalized frequency response of WFPD1 demonstrated in Table 1. In the special case of $Z_S = Z_L = 50\ \Omega$, the initial values of Z_e, Z_o, and Z_1 can be calculated as 158, 60, and 69 Ω based on equation (10). The values of Z_e, Z_o, and $Z_1$are adjusted as 158, 60, and 63 Ω to obtain wider passband BW and equal ripple return loss response.

Analysis of WFPD2 under even-mode excitation

For WFPD2, the loading terminations $Z_{T1}$and Z_{T2} are all implemented as (4) open-circuited stub, while the TL section is selected as (1) quarter-wavelength TL. The expressions of X_{T1} and X_{T2} can be deduced as equation (12) based on the schematic representation of WFPD2 demonstrated in Table 1.

$$X_{T1} = \frac{Z_4 \cot\theta(\tan^2\theta - Z_3/Z_4)}{1 + Z_3/Z_4}, \tag{12a}$$

$$X_{T2} = \frac{Z_6 \cot\theta(\tan^2\theta - Z_5/Z_6)}{1 + Z_5/Z_6}, \tag{12b}$$

$$Z_{INE} = \frac{(Z_e - Z_o)^2 Z_L}{2Z_1^2}. \tag{13}$$

At center frequency f_0, $A_{TL} = D_{TL} = 1/X_{T1} = 1/X_{T2} = 0$. After substituting equations (9a) and (12) into (4), the input impedance in port 1 (Z_{INE}) can be simplified as equation (13) when the WFPD2 is under even-mode excitation. In the special case of $Z_S = Z_L = 50\ \Omega$, the initial values of Z_e, Z_o, and Z_1 can be calculated as 158, 60, and 69 Ω based on equation (13). To realize wider passband BW and equal ripple return loss response, the values ofZ_e, Z_o, Z_1 are tuned as 158, 60, and 63 Ω, respectively.

Combining equations (1–5), (9a), and (12), the frequencies of the TZs below $2f_0$ can be deduced as equation (14). It can be observed from the normalized frequency response that six TZs are introduced below $2f_0$ in WFPD2, which agrees well with equation (14).

$$f_{TZ0} = 0, \tag{14a}$$

$$f_{TZ1} = \frac{2f_0}{\pi}\arctan\sqrt{Z_3/Z_4}, \tag{14b}$$

$$f_{TZ2} = \frac{2f_0}{\pi}\arctan\sqrt{Z_5/Z_6}, \tag{14c}$$

https://doi.org/10.1017/S1759078718001459 Published online by Cambridge University Press

Table 1. Summary of three WFPDs with different kinds of TL sections and loading terminations

WFPD types	WFPD 1			WFPD 2			WFPD 3		
Types of TL section and loading terminations	TL section	Z_{T1}	Z_{T2}	TL section	Z_{T1}	Z_{T2}	TL section	Z_{T1}	Z_{T2}
	(1)	(3)	(4)	(1)	(4)	(4)	(2)	(5)	(4)
Schematic	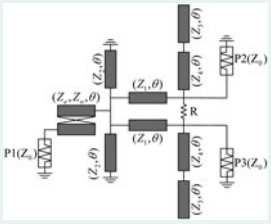			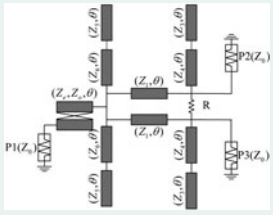			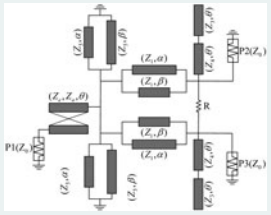		
Layout	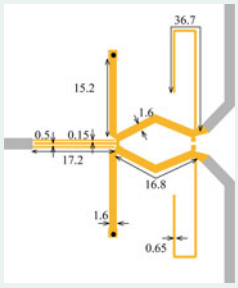			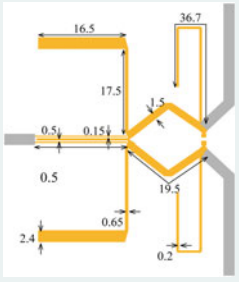			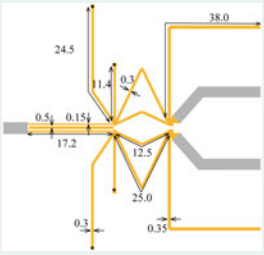		
Photograph	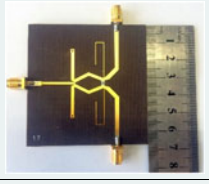			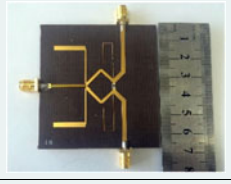			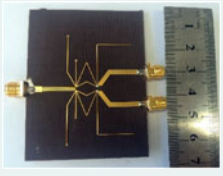		
Normalized frequency response S_{11} S_{21}	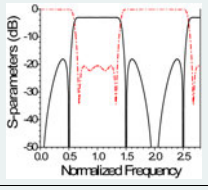			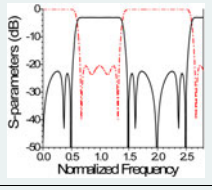			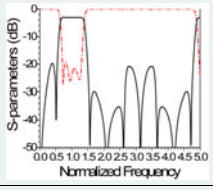		
Frequencies of TZs	0, $0.5f_0$, $1.5f_0$, $2f_0$			0, $0.38f_0$, $0.5f_0$, $1.5f_0$, $1.62f_0$, $2f_0$			0, $0.5f_0$, $1.5f_0$, $2.0f_0$, $2.5f_0$, $3.0f_0$, $3.5f_0$, $4.5f_0$		
Out-of-band rejection performance	>18 dB ($2.4f_0$)			>22 dB ($2.5f_0$)			>20 dB ($4.7f_0$)		
FBW	79.7%			79.0%			74.4%		
Size	$0.48\lambda_g \times 0.65\lambda_g$			$0.48\lambda_g \times 0.68\lambda_g$			$0.7\lambda_g \times 0.7\lambda_g$		

$$f_{TZ3} = 2f_0 - \frac{2f_0}{\pi} \arctan\sqrt{Z_5/Z_6}, \tag{14d}$$

$$f_{TZ4} = 2f_0 - \frac{2f_0}{\pi} \arctan\sqrt{Z_3/Z_4}, \tag{14e}$$

$$f_{TZ5} = 2f_0. \tag{14f}$$

Figure 4 shows the normalized frequency responses of WFPD2 with various values of Z_3, Z_4, Z_1, Z_e, and Z_o. As shown in Fig. 4(a), passband selectivity and passband BW are mainly influenced by the frequencies of f_{TZ1} and f_{TZ2}, which can be adjusted by tuning the impedances of cascade open-circuited stubs (Z_3 and Z_4). The frequency of f_{TZ1} will shift to higher frequency and the frequency of f_{TZ2} will shift to lower frequency when the value of Z_3/Z_4increases, meanwhile the BW will become narrow when the value of Z_3/Z_4 increases. The conclusions came from Fig. 4(a) are in good agreement with equation (14). Apply the same principle to WFPD1, the required passband selectivity and BW could be realized by adjusting the value of Z_3/Z_4, which accords with equation (11).

According to equations (10) and (13), the input impedance of port 1 (Z_{INE}) in WFPD1 and WFPD2 is mainly affected by the values of Z_1, Z_e, and Z_o. Normalized frequency responses of WFPD2 with various values of Z_1, Z_e, and Z_o are shown in Figs 4(b) and 4(c), respectively. Figure 4(b) demonstrates that in-band return loss with constant BW can be optimized by selecting a proper value of Z_1. As observed in Fig. 4(c), the return loss in the passband frequency range is influenced by values of Z_e and Z_o. Thus, excellent in-band return loss in WFPD1 and WFPD2 could be realized by adjusting the values of Z_1, Z_e, and Z_o.

https://doi.org/10.1017/S1759078718001459 Published online by Cambridge University Press

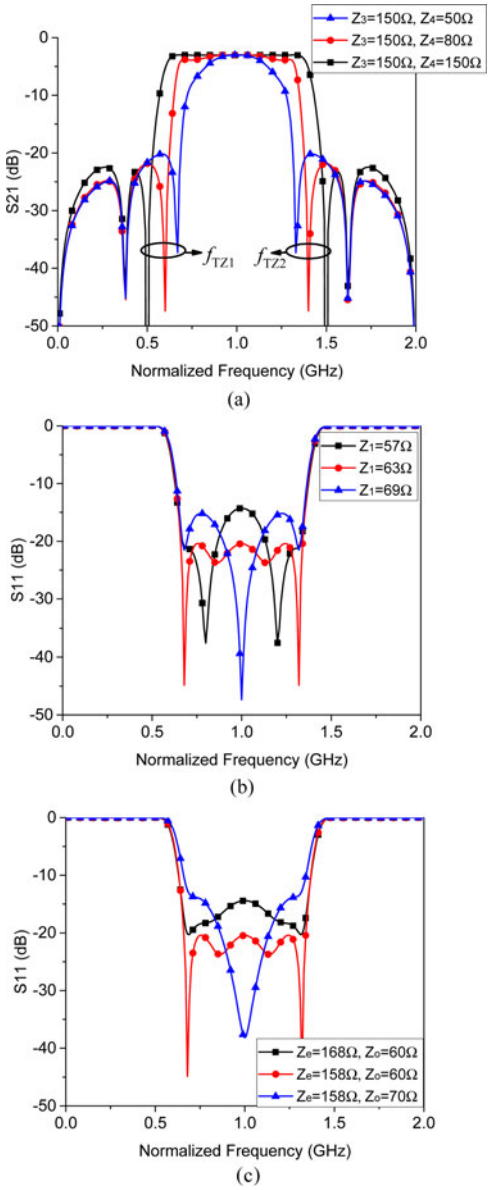

Fig. 4. Normalized frequency responses of WFPD2 with various (a) Z_3 and Z_4, (b) Z_1, (c) Z_e and Z_o.

Analysis of WFPD3 under even-mode excitation

As for WFPD3, the loading termination Z_{T1} is implemented as (5) short-circuited DTLs and the loading termination Z_{T2} is chosen as (4) cascade open-circuited stub, while the TL section is selected as (2) DTLs. The ABCD matrix of the DTLs is demonstrated in equation (15a) which has been presented in paper [21]. X_{T1} and X_{T2} can be expressed as equations (15b) and (15c).

$$\begin{pmatrix} \dfrac{\cos\alpha\sin\beta+\cos\beta\sin\alpha}{\sin\alpha+\sin\beta} & \dfrac{jZ_S\sin\alpha\sin\beta}{\sin\alpha+\sin\beta} \\ jY_S\dfrac{(\cos\alpha-\cos\beta)^2+(\sin\alpha+\sin\beta)^2}{\sin\alpha+\sin\beta} & \dfrac{\cos\alpha\sin\beta+\cos\beta\sin\alpha}{\sin\alpha+\sin\beta} \end{pmatrix}, \tag{15a}$$

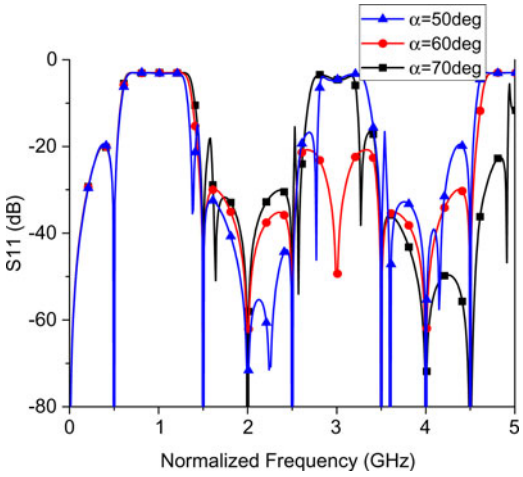

Fig. 5. Normalized frequency responses of WFPD3 with various electrical length (α).

$$X_{T1}=\frac{\tan\alpha+\tan\beta}{Z_5\tan\alpha\cdot\tan\beta}, \tag{15b}$$

$$X_{T2}=\frac{Z_4\cot\theta(\tan^2\theta-Z_3/Z_4)}{1+Z_3/Z_4}. \tag{15c}$$

As shown in Fig. 2, the lengths of DTLs are defined as α, β, and $\alpha+\beta=180^{\circ}$ at f_0. Thus, $A_{TL}=D_{TL}=1/X_{T1}=1/X_{T2}=0$ at f_0. According to equations (4) and (15), input impedance in port 1 (Z_{INE}) could be calculated as equation (16) when WFPD3 is under even-mode excitation. In a special case of $Z_S=Z_L=50\ \Omega$, the initial values of Z_e, Z_o, and Z_1 can be calculated as 150, 60, and 147 Ω based on equation (16). Moreover, the values of Z_e, Z_o, and Z_1 are adjusted as 150, 60, and 136 Ω to obtain wider BW and equal ripple return loss response. In WFPD3, the TZs below $2f_0$ are expressed as equation (17) based on equations (1–5) and (15). The frequencies of TZs in series and parallel DTLs are shown in equation (18), which has been analyzed in our previous work [22]. The normalized frequency response of WFPD3 is depicted in Table 1, which has a good agreement with equations (17 and 18).

$$Z_{INE}=\frac{(Z_e-Z_o)^2((\cos\alpha-\cos\beta)^2+(\sin\alpha+\sin\beta)^2)Z_L}{2Z_1^2\sin\alpha\sin\beta}, \tag{16}$$

$$f_{TZ0}=0, \tag{17a}$$

$$f_{TZ1}=\frac{2f_0}{\pi}\arctan\sqrt{Z_3/Z_4}, \tag{17b}$$

$$f_{TZ2}=2f_0-\frac{2f_0}{\pi}\arctan\sqrt{Z_3/Z_4}, \tag{17c}$$

$$f_{TZ3}=2f_0, \tag{17d}$$

$$f_{TZn}^{S}=\left\{(n+1)f_0\middle|n\in N_+,f>0\middle|\tan\left(\frac{f\alpha}{f_0}\right)=-\tan\left(\frac{f(\pi-\alpha)}{f_0}\right)\right\}, \tag{18a}$$

https://doi.org/10.1017/S1759078718001459 Published online by Cambridge University Press

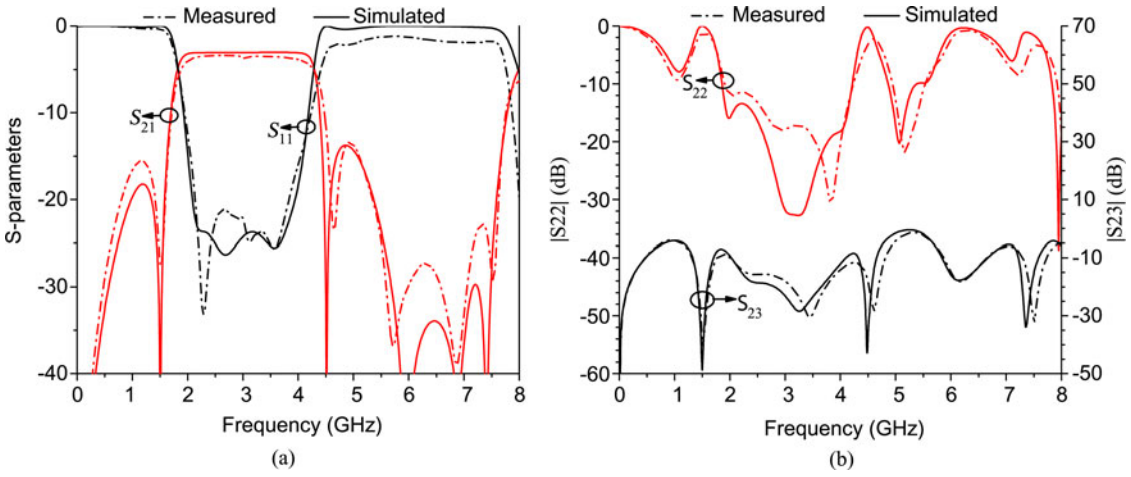

Fig. 6. Simulated and measured results of WFPD1. (a) S_{11} and S_{21}, (b) S_{22} and S_{23}.

$$f_{TZn}^{P} = \left\{ \frac{n\pi f_0}{\alpha}, \frac{n\pi f_0}{(\pi - \alpha)}, n \in N_+ \right\}. \quad (18b)$$

According to equation (16), the return loss of WFPD3 is mainly influenced by the values of Z_e, Z_o, and Z_1. It could be seen from equation (17) that the value of Z_3/Z_4 could be adjusted to obtain required BW and passband selectivity. Figure 5 shows the normalized frequency responses of WFPD3 with various electrical lengths (α). It could be observed from Fig. 5 that TZ could be obtained at $3f_0$ when electrical length (α) is chosen as 60°, which accords to equation (18). The best out-of-band rejection performance could be obtained by defining the electrical length (α) as 60°.

Analysis of three WFPDs under odd-mode excitation

In WFPD1, WFPD2, and WPFD3, $A_{TL} = D_{TL} = 1/X_{T1} = 1/X_{T2} = 0$ at f_0. Under odd-mode excitation, the input impedance in port 2 (Z_{INO}) could be simplified as R/2 based on equation (7).

Simulated and measured results

Discussion about S parameters

To verify the analysis above, the proposed three WFPDs have been constructed on the substrate with a relative dielectric constant of 3.5 and a thickness of 31 mil. The photographs and dimensions (unit: mm) of proposed WFPDs are shown in Table 1.

The EM-simulated and measured results of proposed WFPDs are shown in Figs 6–8. For WFPD1, the measured S_{11} is >20 dB and the minimum insertion loss is 3.4 dB (including power division loss) in the passband, while the 3 dB fractional BW (FBW) is 79.7% from 1.81 to 4.21 GHz. As shown in Fig. 6(a), the measured harmonic suppression is >13.4 dB from 4.5 to 7.7 GHz. It is seen from Fig. 6(b) that measured S_{22} is better than 11.6 dB during the operating band and the measured isolation (S_{23}) is higher than 13 dB from DC to 8 GHz.

For WFPD2, the measured S_{11} is >15 dB and the minimum insertion loss is 3.3 dB (including power division loss) in the passband, while the 3 dB FBW is 79.0% from 1.80 to 4.15 GHz. As shown in Fig. 7(a), the measured harmonic suppression is >17.6 dB from 4.5 to 7.4 GHz. It is observed from Fig. 7(b) that measured $S_{22}$is better than 13 dB during the operating band and the measured isolation (S_{23}) is higher than 12 dB from DC to 8 GHz.

For WFPD3, the measured S_{11} is >15 dB and the minimum insertion loss is 3.5 dB (including power division loss) in the passband, while the 3 dB FBW is 74.4% from 1.90 to 4.15 GHz. As shown in Fig. 8(a), the measured harmonic suppression is >17.0 dB from 4.5 to 14.25 GHz. It is observed from Fig. 8(b) that measured S_{22} is better than 15.5 dB during the operating band and the measured isolation (S_{23}) is higher than 11.5 dB from DC to 15 GHz.

The comparisons between the proposed WFPDs and other published work are summaried in Table 2. Excellent performance including wide FBW, low insertion loss, wide upper stopband range with high attenuation and multiple TZs could be obtained in the proposed WFPDs.

Discussion about power capacity

Coaxial lines and waveguides are usually employed to design microwave components with high power capacity, like high-power PDs [23–25]. Unlike the conventional Wilkinson PD with high power capacity, the proposed WFPD structures are mainly constructed by resonator-based impedance transforming networks which make their power capacity more similar to the resonator-based microstrip filters [26] as well as microstrip antennas [27] with power capacity of several watts. However, the WFPDs in this paper are very attractive to design filtering microstrip antenna arrays or other microstrip transceiver circuits with low-power signals.

Conclusions

A series of WFPDs is proposed in this paper. Various kinds TL sections and loaded stubs are adopted to design different types of WFPDs. The proposed ideas are validated by the good agreement between simulated results and measured results of proposed WFPDs. The proposed three WFPDs have good filtering response and out-of-band rejection performances, which can fulfil the broadband communication requirements. Specifically, in this paper, WFPD1 is introduced with simple design process and compact circuit size to verify the proposed filtering PD structures and analysis. However, WFPD1 suffers from poor out-of-band rejection performance. By replacing short-circuited stubs in WFPD1 with cascade open-circuited stubs, WFPD2 is constructed with improved out-of-band rejection, but WFPD2 has the disadvantage of relative complicated design procedures and larger circuit size. Employing DTLs in WFPD3, the upper stopband frequency range is greatly extended. However, WFPD3 has

https://doi.org/10.1017/S1759078718001459 Published online by Cambridge University Press

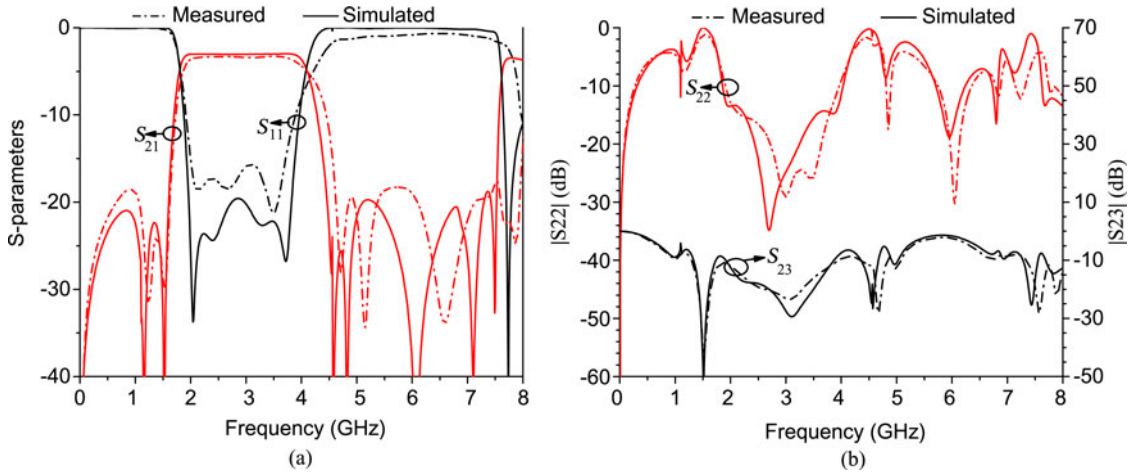

Fig. 7. Simulated and measured results of WFPD2. (a) S_{11} and S_{21}, (b) S_{22} and S_{23}.

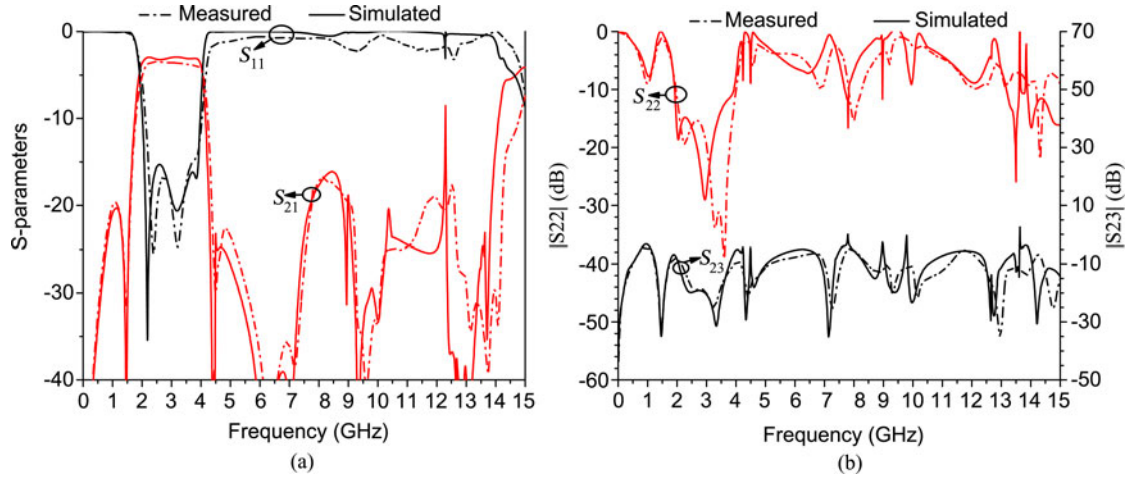

Fig. 8. Simulated and measured results of WFPD3. (a) S_{11} and S_{21}, (b) S_{22} and S_{23}.

Table 2. Comparisons between the proposed WFPDs and other published filtering PDs.

Ref.	f_0 (GHz)	FBW (%)	Insertion loss (dB)	Stopband rejection (dB)	Number of TZs
[4]	0.92	6.5	3.96	$2.6f_0$ ≥25	4
[5]	2.41	7.1	4.2	$2.9f_0$ ≥20	3
[7]	3.75	4	3.75	$2.9f_0$ ≥12	4
[8]	2.45	7.1	4.3	$2.0f_0$ ≥21	3
[9]	2.4	8.3	3.9	$2.7f_0$ ≥23	5
[13]	2.0	75.2	3.5	$2.65f_0$ ≥16	4
[17]	3.0	70	3.3	$2.6f_0$ ≥13	4
[19]	3.0	104.5	3.66	$5.0f_0$ ≥15	3
WFPD1	3.0	79.7	3.4	$2.6f_0$ ≥13.4	4
WFPD2	3.0	79.0	3.3	$2.5f_0$ ≥17.6	6
WFPD3	3.0	74.4	3.5	$4.75f_0$ ≥17	8

the largest circuit size and most complicated design procedures. In the practical application, according to the requirements of circuit size, harmonic suppression performance as well as upper stopband BW, the sufficient WFPD type can be selected.

Acknowledgement. This work was supported in part by the National Natural Science Foundations of China (No. 61327806 and No. 61422103), in part by the National Basic Research Program of China (973 Program) under Grant 2014CB339900, and in part by 863 Program under Grant 2015AA016801.

https://doi.org/10.1017/S1759078718001459 Published online by Cambridge University Press

References

1. **Burdin F, Podevin F and Ferrari P** (2016) Flexible and miniaturized power divider. *International Journal of Microwave and Wireless Technologies* **8**, 547–557.
2. **Karimi G, Siahkamari H and Hamedani F** (2015) A novel miniaturized Gysel power divider using lowpass filter with harmonic suppression. *International Journal of Electronics and Communications* **69**, 856–860.
3. **Zhang XY, Wang KX and Hu BJ** (2013) Compact filtering power divider with enhanced second-harmonic suppression. *IEEE Microwave and Wireless Components Letters* **23**, 483–485.
4. **Song K** (2015) Compact filtering power divider with high frequency selectivity and wide stopband using embedded dual-mode resonator. *Electronics Letters* **51**, 495–497.
5. **Danaeian M, Moznebi AR, Afrooz K and Hakimi A** (2017) Miniaturized filtering SIW power divider with arbitrary power-dividing ratio loaded by open complementary split-ring resonators. *International Journal of Microwave and Wireless Technologies* **9**, 1827–1832.
6. **Ren X, Song KJ, Hu BK and Chen QK** (2014) Compact filtering power divider with good frequency selectivity and wide stopband based on composite right-/left-handed transmission lines. *Microwave and Optical Technology Letters* **56**, 2122–2125.
7. **Song KJ, Ren X, Chen FL and Fan Y** (2013) Compact in-phase power divider integrated filtering response using spiral resonator. *IET Microwaves, Antennas & Propagation* **8**, 228–234.
8. **Zhang B, Yu C and Liu Y** (2016) Compact power divider with bandpass response and improved out-of-band rejection. *Journal of Electromagnetic Waves and Applications* **30**, 1124–1132.
9. **Song K, Zhou YF, Fan MY, Zhu Y and Fan Y** (2017) Wide-stopband bandpass-filtering power divider with high-frequency selectivity. *International Journal of Microwave and Wireless Technologies* **9**, 1931–1936.
10. **Wang X, Wang J and Zhang G** (2016) Design of wideband filtering power divider with high selectivity and good isolation. *Electronics Letters* **52**, 1389–1391.
11. **Wong SW and Zhu L** (2009) Ultra-wideband power dividers with good isolation and improved sharp roll-off skirt. *IET Microwaves, Antennas & Propagation* **3**, 1157–1163.
12. **Chen SY, Zhang DS and Yu YT** (2013) Wideband SIW power divider with improved out-of-band rejection. *Electronics Letters* **49**, 943–944.
13. **Tang C, Lin XQ, Fan Y and Song KJ** (2016) A wideband power divider with bandpass response. *International Journal of Microwave and Wireless Technologies* **8**, 583–590.
14. **Gao X, Feng WJ, Che WQ and Xue Q** (2017) Wideband balanced-to-unbalanced filtering power dividers based on coupled lines. *IEEE Transactions on Microwave Theory and Techniques* **65**, 86–95.
15. **Zhu H, Abbosh AM and Guo L** (2016) Wideband four-way filtering power divider with sharp selectivity and wide stopband using looped coupled-line structures. *IEEE Microwave and Wireless Components Letters* **26**, 413–415.
16. **Song K, Mo Y and Fan Y** (2014) Wideband four-way filtering-response power divider with improved output isolation based on coupled lines. *IEEE Microwave and Wireless Components Letters* **24**, 674–676.
17. **Zhang B and Liu Y** (2015) Wideband filtering power divider with high selectivity. *Electronics Letters* **51**, 1950–1952.
18. **Moradi E, Moznebi AR, Afrooz K and Movahhedi M** (2018) Gysel power divider with efficient second and third harmonic suppression using one resistor. *International Journal of Electronics and Communications* **89**, 116–122.
19. **Tang CW and Chen JT** (2016) A design of 3-dB wideband microstrip power divider with an ultra-wide isolated frequency band. *IEEE Transactions on Microwave Theory and Techniques* **64**, 1806–1811.
20. **Tang CW, Tseng CT, Chiu SH and Wu PH** (2013) Design of wide pass-band/stopband microstrip bandpass filters with the stepped coupled line. *IEEE Transactions on Microwave Theory and Techniques* **61**, 1095–1103.
21. **Tang CW, Chen MG and Tsai CH** (2008) Miniaturization of microstrip branch-line coupler with dual transmission lines. *IEEE Microwave and Wireless Components Letters* **18**, 185–187.
22. **Zhang B, Wu YL, Yu CP and Liu Y** (2016) Miniaturised wideband band-pass filter based on harmonic suppressed dual transmission lines. *Electronics Letters* **52**, 734–736.
23. **Guo LT, Li JW, Huang WH, Shao H and Ba T** (2017) A compact four way power combiner. *IEEE Microwave and Wireless Components Letters* **27**, 239–241.
24. **Guo LT, Li JW, Huang WH, Shao H, Ba T, Xie SY, Jiang Y and Deng GJ** (2018) Design of compact high isolation four way power combiners. *IEEE Transaction Microwave Theory Techniques* **66**, 2185–2198.
25. **Guo LT, Li JW, Huang WH, Shao H, Ba T, Jiang TY, Jiang Y and Deng GJ** (2017) A waveguide magic-T with coplanar arms for high-power solid-state power combining. *IEEE Transaction Microwave Theory Techniques* **65**, 2942–2952.
26. **Endo Y, Ono S, Uno M, Satio T, Satio A, Nakajima K and Ohshima S** (2011) Improvement in power-handling capability of superconducting filters using multi-layered microstrip line resonators. *IEEE Transactions on Applied Superconductivity* **21**, 559–562.
27. **Pozar DM** (1983) Considerations for millimeter wave printed antennas. *IEEE Transactions on Antennas and Propagation* **31**, 740–747.

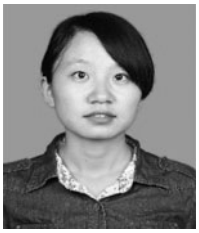

Gaoya Dong was born in Shanxi, China, in 1993. She received the B.S. degree in Applied Physics from Xidian University, Xi 'an, China, in 2015. She is currently pursuing the Ph.D. degree in Electrical Engineering in Beijing University of Posts and Telecommunications, Beijing, China. Her current research interests include planar microwave power dividers and antennas.

Weimin Wang was born in Shandong, China, in 1977. She received the B.Eng. degree in Telecommunication Engineering, the M.Sc. degree in Electromagnetics and Microwave Technology, and the Ph.D. degree in Electronic and Information Engineering from the Beijing University of Posts and Telecommunications, Beijing, China, in 1999, 2004, and 2014, respectively.

Bo Zhang was born in Shanxi, China, in 1991. He received the B.S. and M.S. degrees all in Electronic and Information Engineering from Beijing University of Posts and Telecommunications (BUPT), Beijing, China, in 2012 and 2015, respectively, where he is currently working toward Ph.D. degree in electrical engineering. His current research interests include planar microwave filters, power divider, antennas, and power amplifiers.

Yuanan Liu received the B.E., M.Eng., and Ph.D. degrees in Electrical Engineering from the University of Electronic Science and Technology of China, Chengdu, China, in 1984, 1989, and 1992, respectively. In 1984, he joined the 26th institute of Electronic Ministry of China to develop the inertia navigating system. In 1992, he began his first post-doctor position in EMC laboratory of Beijing University of Posts and Telecommunications (BUPT), Beijing, China. In 1995, he started his second post-doctor in broadband mobile laboratory of Department of System and Computer Engineering, Carleton University, Ottawa, Canada. From July, 1997, as a professor, he is with wireless communication center of College of Telecommunication Engineering, BUPT, Beijing, China, where he is involved in the development of next-generation cellular system, wireless LAN, Bluetooth application for data transmission, EMC design strategies for high-speed digital system, and EMI and EMS measuring sites with low cost and high performance.

https://doi.org/10.1017/S1759078718001459 Published online by Cambridge University Press